Single-crystal neutron diffraction study of Nd magnetic ordering in $NdFeO_3$ at low temperature

J. Bartolomé, E. Palacios, M. D. Kuz'min, and F. Bartolomé
Instituto de Ciencia de Materiales de Aragón, CSIC-Universidad de Zaragoza, 50009 Zaragoza, Spain

I. Sosnowska and R. Przeniosło
Institute of Experimental Physics, Warsaw University, PL-00 681 Warsaw, Poland

R. Sonntag
Hahn-Meitner-Institut, D-14109 Berlin, Germany

M. M. Lukina
Department of Physics, Moscow State University, Leninskie Gory, 119899 Moscow, Russia
(Received 2 August 1996; revised manuscript received 19 November 1996)

The temperature variation of the (100) and (010) neutron diffraction peak intensities, related only to the Nd magnetic moments, have been measured on a $NdFeO_3$ single crystal, at temperatures down to 70 mK. The (100) peak becomes noticeable below 25 K while the (010) peak only gives an appreciable contribution below 1 K. Above $T_{N2} \approx 1$ K the (100) peak intensity is accounted for by the electronic magnetic moments polarized by the Nd-Fe exchange field. Near T_{N2} a change of slope is observed in the temperature dependence of the (100) reflection intensity, demonstrating the crossover from the above polarization of Nd under the Nd-Fe exchange to proper long-range ordering due to Nd-Nd interaction. Below ~ 0.4 K another mechanism, polarization of Nd nuclear moments by hyperfine field, contributes to the intensity of the (100) and (010) peaks. A simple mean-field model explains consistently the observed temperature dependence of the diffraction intensities as well as earlier specific-heat data. The main feature of this model is allowance for Van Vleck susceptibility, which appears to play an important role in the overall polarization of Nd. The values of the hyperfine field at the Nd nuclei $H_{\rm hf} = 1.0 \pm 0.15$ MOe and of the Nd electronic magnetic moment $\mu_{\rm Nd} = 0.9\ \mu_B$ are deduced, the ratio $H_{\rm hf}/\mu_{\rm Nd}$ being the same as in other Nd compounds. [S0163-1829(97)11817-3]

I. INTRODUCTION

Perovskites in general and rare-earth orthoferrites $RFeO_3$ in particular are recognized model systems in solid-state physics and as such they have been under thorough investigation over decades. Many techniques have been applied and among them neutron diffraction has been used extensively to determine the magnetic structures of the orthoferrites, starting with the pioneer work of Koehler *et al.* back in 1960,[1] where, among others, $NdFeO_3$ was studied. It thus came as a surprise when two years ago in this by then well-studied compound the moments of Nd were found to undergo a collective magnetic ordering at $T_{N2} = 1.05$ K^2, not just unnoticed, but regarded as impossible before.[3]

$NdFeO_3$ has an orthorhombically distorted perovskite structure, space group $D_{2h}^{16} - Pbnm$, with four formula units per elementary cell.[4,5] The magnetic configurations are customarily described in terms of eigenstates of linear combinations of spin operators for different rare-earth or iron sites,[6] whose Cartesian components transform as one of the eight one-dimensional irreducible representations of the reduced space group $\widetilde{D}_{2h}^{16}$. For the Nd subsystem these linear combinations are

$$\hat{\mathbf{f}} = \hat{\mathbf{s}}_1 + \hat{\mathbf{s}}_2 + \hat{\mathbf{s}}_3 + \hat{\mathbf{s}}_4, \tag{1}$$

$$\hat{\mathbf{a}} = \hat{\mathbf{s}}_1 - \hat{\mathbf{s}}_2 - \hat{\mathbf{s}}_3 + \hat{\mathbf{s}}_4,$$

$$\hat{\mathbf{g}} = \hat{\mathbf{s}}_1 - \hat{\mathbf{s}}_2 + \hat{\mathbf{s}}_3 - \hat{\mathbf{s}}_4,$$

$$\hat{\mathbf{c}} = \hat{\mathbf{s}}_1 + \hat{\mathbf{s}}_2 - \hat{\mathbf{s}}_3 - \hat{\mathbf{s}}_4,$$

where $\hat{\mathbf{s}}_1$, $\hat{\mathbf{s}}_2$, $\hat{\mathbf{s}}_3$, and $\hat{\mathbf{s}}_4$ are the electronic spins of the four Nd^{3+} ions situated approximately at $(0,0,\frac{1}{4})$, $(0,0,\frac{3}{4})$, $(\frac{1}{2},\frac{1}{2},\frac{3}{4})$, and $(\frac{1}{2},\frac{1}{2},\frac{1}{4})$ in the unit cell. Formulas similar to Eq. (1), but with iron spins, define operators $\hat{\mathbf{F}}$, $\hat{\mathbf{A}}$, $\hat{\mathbf{G}}$, and $\hat{\mathbf{C}}$ used to describe magnetic configurations of iron.

The iron spins in $NdFeO_3$ order at high temperature, $T_{N1} = 690$ K;[7] the magnetic structure is antiferromagnetic, with a weakly ferromagnetic component G_xF_z (irreducible representation Γ_4). Between 125 and 167 K the iron spins rotate continuously in the ac plane, from G_xF_z to G_zF_x ($\Gamma_4 - \Gamma_2$).[8] At low temperatures the G_zF_x (Γ_2) spin configuration of iron induces, via Nd-Fe exchange, a noticeable Nd polarization of the same symmetry Γ_2 (c_yf_x). The weak ferromagnetic moments, F_x of iron and f_x of Nd, are antiparallel and at $T = 8$ K the overall spontaneous magnetization becomes compensated.[9,10] Both the G_z mode of iron and the c_y mode of Nd were observed in powder neutron diffraction experiments at low temperatures.[11,12]

The proper magnetic ordering of Nd in $NdFeO_3$ takes place at $T_{N2} = 1.05$ K, as manifested by a sharp peak in the specific heat, found recently[2] on the low-temperature slope of the Schottky anomaly known from an earlier work.[3] The interpretation of the peak was based upon the analogy with other orthoferrites, $GdFeO_3$ (Ref. 13) and $DyFeO_3$ (Ref. 14),

as well as with isostructural Nd compounds, $NdGaO_3$ (Ref. 15) and $NdCoO_3$, (Ref. 2) where similar magnetic ordering had been observed before. The specific-heat data were successfully described by the mean-field model,[2] which, however, due to its disregard of important effects associated with Van Vleck susceptibility, proved insufficient for the neutron diffraction peak intensities dealt with in the present work.

Thus, our primary objective is to gain information about the magnetic symmetry of the Nd subsystem in the ordered phase. Secondly, we shall revise the mean-field model of Ref. 2 so as to allow for the Van Vleck contribution, with a view to providing a coherent description of both the specific-heat and neutron diffraction data. Finally, below 1 K we expect to see the contribution from the Nd nuclei polarized by the hyperfine field, as was observed in $NdGaO_3$,[16] so we shall include this effect in the model.

II. EXPERIMENTAL DETAILS

The single crystal was grown by the flux method. Spontaneous crystallization of $NdFeO_3$ took place under isothermic evaporation of a solution of stoichiometric mixture of Nd_2O_3 and Fe_2O_3 in PbO-PbF_2-B_2O_3 melt. The crystal had natural perovskite habit with faces parallel to (110), (110), and (001). It was checked optically and with x-ray diffraction; no twins were detected within the experimental sensitivity.

The diffraction experiment was performed on the double axis diffractometer E4 at the Neutron Scattering Center of the Hahn-Meitner-Institut in Berlin. The high-resolution mode was employed with a wavelength of $\lambda = 2.45$ Å. A $\lambda/2$ pyrolitic graphite filter was used in all the experiments. Two setups were used: a ^{3}He-^{4}He refrigerator coupled to a standard ILL ^{4}He gas-flow ''orange'' cryostat between 70 mK and 2 K, and just the ''orange'' cryostat from 2 to 30 K. The sample was oriented with its c axis vertical; it was glued with Stycast resin on a vertical thin copper plate placed below a copper rod attached to the refrigerator mixing chamber. The temperature was measured at the mixing chamber, so a certain temperature gradient between the sample and thermometer was expected.

Once the sample was cooled down to 1 K, the intensities of the purely nuclear reflections (110) and (110) were measured in θ-2θ scans to verify the sample orientation and to obtain an absolute reference for the determination of magnetic intensities. After this, θ-2θ scans were done through the (100) and (010) magnetic positions, at various stabilized temperatures. These scans were fitted to a simple Gaussian function plus a constant background, and from each fitted curve the integrated intensity was evaluated. The scale factor was determined from these intensities at $T = 1.2$ and 5 K. The intensities of the (110) and (110) reflections differed from each other by 15%, probably because of the difference in the absorption of the Cu support plate for different orientations. The magnetic intensities measured at the same temperature with the two cryostats differed by 10%. With just one reflection intensity [that for (110)] available, possible extinction could not be allowed for. So, the absolute accuracy of our measurements is 15%. On the other hand, the relative variations in the peak intensities due to temperature variation were determined better than 1%, as we assured by collecting the data long enough to gain sufficient statistics, and verified by reproducing some of the points.

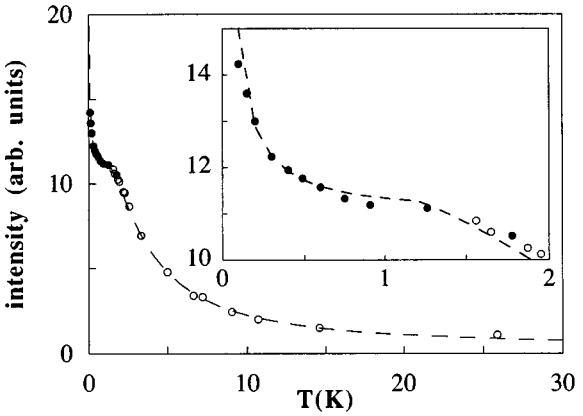

FIG. 1. Temperature dependence of the (100) reflection intensity: ● low-temperature data set; ○ high-temperature data set; dashed curve is a guide for the eye.

III. EXPERIMENTAL RESULTS

In Fig. 1 we present the (100) peak intensity as a function of the temperature, with the two different data sets overlapping between 1.2 and 2 K. As temperature decreases, the following four features become apparent. (a) Between 27 and 1.3 K the intensity continuously grows, as would be expected, due to the progressive polarization of the paramagnetic subsystem of Nd moments under the exchange field created by the Fe ions. (b) A change of slope occurs at $T \approx 1.3$ K, near the Nd ordering temperature $T_{N2} = 1.05$ K. (c) The intensity flattens out between T_{N2} and 800 mK; (d) from 800 mK down to the lowest temperature achieved, 70 mK, the intensity increases steeply; this marks the onset of polarization of the Nd nuclear moments. The electronic magnetic moment of Nd deduced from the total intensity of the (100) peak at $T = 1$ K is $\mu_{\mathrm{Nd}} = 0.9 \pm 0.1 \mu_B$.

In Fig. 2 we show the temperature dependence of the intensity of the (010) peak. Between 27 and 5 K there is a very small peak in the θ-2θ scans that could be due to $\lambda/2$ contamination, so we regard the intensity of this peak as zero

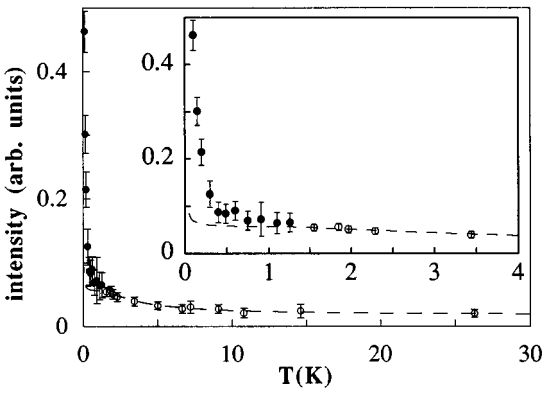

FIG. 2. Temperature dependence of the (010) reflection intensity: ● low-temperature data set; ○ high-temperature data set; dashed curve is 0.06 times the (100) line intensity (ascribed to twins, see text for details).

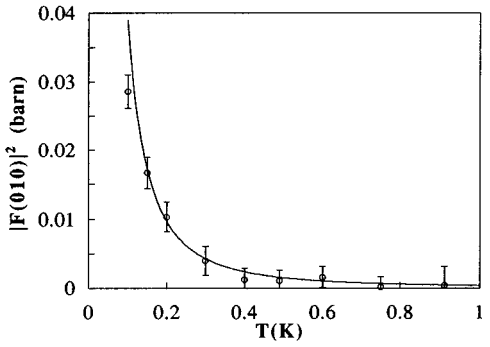

FIG. 3. Temperature dependence of the (010) reflection intensity corrected for twinning. Continuous line was calculated using Eq. (36) with $H_{\rm hf}=1.0$ MOe.

base line for the intensity at lower temperatures. Below 8 K the (010) line intensity starts to grow. This cannot be due to either the long-range ordering of Nd (which would give contribution only below $T_{N2}=1.05$ K) or $\lambda/2$ contamination (which has already been determined at higher temperatures and should remain independent of temperature).

The most plausible explanation for this is that a small volume of the sample is a twin crystal whose *a* axis is parallel to the *b* axis of the main crystal whereas the *c* axes of both coincide. Then the (010) line is contaminated with the intensity of the stronger magnetic (100) peak in an amount proportional to the twin volume. In fact, twinning is virtually inevitable in light rare-earth orthoferrites because their lattice parameters *a* and *b* are nearly equal. When scaled down to 0.06 of its original magnitude, the (100) intensity matches the temperature-dependent part of the (010) intensity above T_{N2}, see Fig. 2. We thus conclude that the twin volume is about 6%, which is too small to be detected with the techniques we used in our preliminary tests.

We subtracted the temperature-independent $\lambda/2$ contribution as well as the twinning contribution [=0.06 times the (100) peak intensity] from the original intensity of the (010) peak and plotted the thus corrected data in Fig. 3. There still remains a residual intensity below 1 K which must be caused by polarization of the Nd nuclei.

We did not attempt to measure the f_x component known to be present above T_{N2} since the corresponding magnetic Bragg peaks are superimposed by the much more intense nuclear peaks.

IV. ANALYSIS

The single-crystal neutron diffraction intensity corresponding to Bragg peak (hkl), or to vector $\tau=\{2\pi h/a,2\pi k/b,2\pi l/c\}$ of reciprocal lattice, is proportional to

$$L(\tau)[|F^n(\tau)|^2+|\mathbf{F}^{m+h}(\tau)|^2], \tag{2}$$

where $L(\tau)$ is the Lorentz factor,[17] $L(100)=L(010)=2.27$, $F^n(\tau)$ is the nuclear structure factor, and $\mathbf{F}^{m+h}(\tau)$ is the magnetic and hyperfine structure factor. For nonpolarized incident neutrons,

$$F^n(\tau)=\sum_{\mathbf{d}} b_{\mathbf{d}c}\mathbf{e}^{i\tau\cdot\mathbf{d}},$$

$$\mathbf{F}^{m+h}(\tau)=\sum_{\mathbf{d}}\left[-\alpha f_{\mathbf{d}}(\tau)\langle\hat{\mathbf{M}}_{\mathbf{d}\perp}\rangle+\frac{b_{di}}{\sqrt{I_{\mathbf{d}}(I_{\mathbf{d}}+1)}}\langle\hat{\mathbf{I}}_{\mathbf{d}}\rangle\right]e^{i\tau\cdot\mathbf{d}}, \tag{3}$$

where the sum is extended over all atoms in a unit cell specified by their position $\mathbf{d}$, $\hat{\mathbf{M}}_{\mathbf{d}\perp}$ is the perpendicular to τ component of the (vector) operator of total electronic magnetic moment of the atom placed at $\mathbf{d}$, and $\hat{\mathbf{I}}_{\mathbf{d}}$ is its nuclear spin operator; $b_{\mathbf{d}c}$ and $b_{\mathbf{d}i}$ are, respectively, the coherent and incoherent scattering lengths and $f_{\mathbf{d}}(\tau)$ is the magnetic form factor for the atom at $\mathbf{d}$; $\alpha=2.695\times10^{-13}$ cm is the magnetic scattering length; $\langle\cdots\rangle$ stands for thermal average. (We have introduced a minus before the electronic magnetic moment anticipating further application to ^{143}Nd and ^{145}Nd, whose nuclear magnetic moments are antiparallel to the corresponding nuclear spins **I**, but parallel to the hyperfine field and the electronic magnetic moments **M** producing that field.)

We shall herein focus on the (100) and (010) reflections. Carrying out the summation in Eqs. (3), with the atom positions $\mathbf{d}$ for $NdFeO_3$ we find that both $F^n(100)$ and $F^n(010)$ vanish, whereas the only nonzero contribution to $\mathbf{F}^{m+h}(100)$ and $\mathbf{F}^{m+h}(010)$ comes from the four Nd atoms. Taking into account that for Nd^{3+} $f(100)=f(010)=0.93$,[18] we write $\mathbf{F}^{m+h}(100)$ as follows:

$$\mathbf{F}^{m+h}(100)=0.93\alpha\langle\hat{\mathbf{M}}_{1\perp}+\hat{\mathbf{M}}_{2\perp}-\hat{\mathbf{M}}_{3\perp}-\hat{\mathbf{M}}_{4\perp}\rangle$$
$$-\frac{b_{\mathrm{Nd},i}}{\sqrt{I(I+1)}}\langle\hat{\mathbf{I}}_1+\hat{\mathbf{I}}_2-\hat{\mathbf{I}}_3-\hat{\mathbf{I}}_4\rangle, \tag{4}$$

where the vector operator $\hat{\mathbf{M}}_{\perp}=\{0,\hat{M}_y,\hat{M}_z\}$ has only *y* and *z* components. The expression for $\mathbf{F}^{m+h}(010)$ is identical with Eq. (4), but $\hat{\mathbf{M}}_{\perp}$ then means $\{\hat{M}_x,0,\hat{M}_z\}$. Thus, $\mathbf{F}^{m+h}$ for both reflections under study contains operators similar to the spin operator $\hat{\mathbf{c}}$ defined by Eqs. (1). This means that a nonzero magnetic part of $\mathbf{F}^{m+h}(100)$ can only result from magnetic configurations of type c_y (Γ_2) and/or c_z (Γ_1), whereas $\mathbf{F}^{m+h}(010)$ can only receive magnetic contributions from configurations of type $c_x(\Gamma_3)$ and/or c_z; however, any *c*-type configuration of nuclear moments contributes to the intensity of both peaks. A purely hyperfine (010) peak and a (100) peak with a strong magnetic component, observed in the present work as well as in Ref. 19, suggest that the observed mode is c_y. Then $\mathbf{F}^{m+h}$ has only a *y* component, given by

$$F^{m+h}(010)=-\frac{b_{\mathrm{Nd},i}}{\sqrt{I(I+1)}}\langle\hat{I}_{1y}+\hat{I}_{2y}-\hat{I}_{3y}-\hat{I}_{4y}\rangle, \tag{5}$$

$$F^{m+h}(100)=0.93\alpha\times4Sg_y\eta_2$$
$$-\frac{b_{\mathrm{Nd},i}}{\sqrt{I(I+1)}}\langle\hat{I}_{1y}+\hat{I}_{2y}-\hat{I}_{3y}-\hat{I}_{4y}\rangle, \tag{6}$$

where η_2 is a dimensionless parameter describing magnetic order of type $c_y(\Gamma_2)$,

$$\eta_2=(4Sg_y\mu_B)^{-1}\langle\hat{M}_{1y}+\hat{M}_{2y}-\hat{M}_{3y}-\hat{M}_{4y}\rangle, \quad (7)$$

g_y is the splitting factor for the ground doublet of Nd^{3+}, $S=\frac{1}{2}$ (see the next section).

In principle, intensities of both peaks can also be affected by a-type magnetic modes; however, this is neglected in Eqs. (4)–(7). There are two grounds for such neglect: first, the corresponding terms contain a small prefactor proportional to the deviation of the atomic positions **d** from those characteristic of the ideal perovskite structure; for the ideal perovskite structure these terms vanish completely. Secondly, no noticeable (001) peak was observed in powder neutron diffraction above or below T_{N2},[20] meaning that any possible content of either a_x or a_y mode is negligibly small.

A. Electronic contribution

In this section the temperature dependence of the parameter η_2 defined by Eq. (7) will be calculated. We shall use the mean field approximation, in particular the Nd-Fe exchange will be described by means of a staggered exchange field $H_{\rm ex}$ produced by Fe and acting on the Nd ions. In the temperature range under study this field can be assumed independent of temperature, as the iron magnetic subsystem is fully saturated.

The low-symmetry (point group C_s-m) crystal field splits the $^4I_{9/2}$ multiplet of Nd^{3+} into five Kramers doublets, the first excited doublet being situated as high as at 122 K from the ground state.[21] In the low-temperature range studied in the present work only the lowest doublet is appreciably populated. This enables us to employ the effective spin-$\frac{1}{2}$ formalism. Thus, $\hat{\mathbf{s}}_{\mathbf{d}}$ in Eqs. (1) should be understood as spin operators for $S=\frac{1}{2}$.

The origin of polarization η_2 of the Nd^{3+} ions is twofold: (i) Zeeman splitting of the ground doublet produced by the Nd-Fe and Nd-Nd exchange fields; (ii) Van Vleck susceptibility and associated extra moments induced on the Nd^{3+} ion by the exchange fields. We therefore write

$$\eta_2=-\tfrac{1}{2}\langle\hat{c}_y\rangle+\text{Van Vleck contribution}. \quad (8)$$

Parameter η_2 describes the magnetic mode that transforms like c_y, i.e., it belongs to the irreducible representation Γ_2 of the reduced space group $\tilde{D}_{2h}^{16}$. There exists another spin operator that belongs to Γ_2, $\hat{f}_x$.[6] It is associated with the weak ferromagnetic component of the Nd magnetic configuration, which is very small as compared c_y. It is neglected in the present work, implying that the Nd-Fe exchange field $H_{\rm ex}$ has a nonzero component only in the y direction and that the Nd g tensor has no nondiagonal component g_{xy}.

To describe the proper magnetic ordering of Nd, we introduce another parameter η, which is assumed to belong to a yet unknown irreducible representation Γ_i, $i\neq 2$. For simplicity, we shall limit ourselves to just the Zeeman part of this parameter, $\eta=-\frac{1}{2}\langle\hat{R}\rangle$, where $\hat{R}$ is one of the spin operators of type (1), whose exact form is not yet known. We also assume that any other mode that could possibly belong to the same representation Γ_i remains negligibly small, so that the ordering of Nd can be described with just one order parameter η.

After these preliminaries we write the following mean-field Hamiltonian for Nd ions in one unit cell:

$$\hat{H}_{\rm MF}=-2\theta\eta\hat{R}-2\theta_2\eta_2\hat{c}_y+g_y\mu_B H_{\rm ex}\hat{c}_y - \frac{2}{N}\chi_{VV}\left(H_{\rm ex}+\frac{2\theta_2}{g_y\mu_B}\eta_2\right)^2-2\theta\eta^2-2\theta_2\eta_2^2. \quad (9)$$

In this expression the first and second terms describe the Nd-Nd exchange, modes Γ_i and Γ_2, respectively, and θ and θ_2 are the corresponding exchange constants. The third term corresponds to the Zeeman part of the Nd-Fe interaction. The fourth term takes into consideration the Van Vleck contribution from both the Nd-Fe and Nd-Nd interactions. The fifth and sixth terms correspond to the self-interaction correction. ($N=1.70\times10^{22}$ cm^{-3} is the concentration of Nd ions.)

The free energy splits into four equal free energies (one for each Nd ion in the cell)

$$F=\tfrac{1}{2}\theta\eta^2+\tfrac{1}{2}\theta_2\eta_2^2-T\ln\left[2\cosh\left(\frac{\Delta}{2T}\right)\right] - \frac{\chi_{VV}}{2N}\left(H_{\rm ex}+\frac{2\theta_2}{g_y\mu_B}\eta_2^2\right)^2, \quad (10)$$

where

$$\Delta=[(2\theta\eta)^2+(g_y\mu_B H_{\rm ex}+2\theta_2\eta_2)^2]^{1/2} \quad (11)$$

is the exchange splitting of the Nd^{3+} ground doublet. Minimizing F with respect on η and η_2, one gets the following characteristic equations:

$$\eta=\eta\frac{2\theta}{\Delta}\tanh\left(\frac{\Delta}{2T}\right), \quad (12)$$

$$\eta_2=\frac{\mu_B g_y H_{\rm ex}+2\theta_2\eta_2}{\Delta}\tanh\left(\frac{\Delta}{2T}\right)+\eta_0+\kappa\eta_2, \quad (13)$$

where

$$\eta_0=\frac{2\chi_{VV}H_{\rm ex}}{Ng_y\mu_B}, \quad \kappa=\frac{4\chi_{VV}\theta_2}{Ng_y^2\mu_B^2}. \quad (14)$$

The first term on the right-hand side of Eq. (13) is the Zeeman part of η_2, whereas the following two terms represent the contribution due to the Van Vleck susceptibility.

The entropy of the Nd electronic spin system can be expressed as follows:

$$S=-\frac{\partial F}{\partial T}-\frac{\partial F}{\partial\eta}\frac{\partial\eta}{\partial T}-\frac{\partial F}{\partial\eta_2}\frac{\partial\eta_2}{\partial T}. \quad (15)$$

However, by virtue of the equilibrium conditions $\partial F/\partial\eta=0$ and $\partial F/\partial\eta_2=0$, i.e., one needs to take into account only the explicit dependence of F on T. Carrying out such differentiation of Eq. (10), we get (in units of R per mole)

$$S=\ln 2+\ln\left[\cosh\left(\frac{\Delta}{2T}\right)\right]-\frac{\Delta}{2T}\tanh\left(\frac{\Delta}{2T}\right). \quad (16)$$

Let us discuss the characteristic Eqs. (12) and (13) in some greater detail. There are two distinct possibilities: (i) there is polarization but no proper magnetic order of Nd ($\eta=0$) or (ii) there is proper long-range order ($\eta\neq 0$).

(i) $\eta=0 (T>T_{N2})$. Equation (12) is automatically satisfied, whereas Eq. (14) takes the following form:

$$\sigma=\tanh\left(\frac{\Delta}{2T}\right), \tag{17}$$

where

$$\sigma=(1-\kappa)\,\eta_2-\eta_0, \tag{18}$$

$$\Delta=g_y\mu_B H_{\rm ex}+2\,\theta_2\,\eta_2. \tag{19}$$

Here we have introduced, for convenience, an explicit notation σ for the Zeeman part of the polarization η_2. Using Eqs. (17)–(19) one can rewrite Eq. (16) as follows:

$$S=\ln 2-\tfrac{1}{2}[(1+\sigma)\ln(1+\sigma)+(1-\sigma)\ln(1-\sigma)]. \tag{20}$$

Thus, explicit dependence of S on T has been eliminated; the only source of temperature dependence in Eq. (20) is σ. It is convenient to introduce the following dimensionless variables:

$$t=T\,\frac{\kappa-1}{\theta_2}, \tag{21}$$

$$\delta=\frac{g_y\mu_B H_{\rm ex}(\kappa-1)}{2\,\theta_2}-\eta_0=-\frac{\eta_0}{\kappa}, \tag{22}$$

and to rewrite Eq. (17) in the form resolved for t,

$$t=\frac{2(\delta-\sigma)}{\ln\left(\dfrac{1+\sigma}{1-\sigma}\right)}. \tag{23}$$

This will enable us to calculate the specific heat in a straightforward way,

$$C=T\,\frac{\partial S}{\partial T}=t\,\frac{\partial S/\partial\sigma}{\partial t/\partial\sigma}. \tag{24}$$

Carrying out the necessary derivations of Eqs. (20) and (23) we get

$$C=\frac{(\delta-\sigma)^2(1-\sigma^2)}{t(t+1-\sigma^2)}. \tag{25}$$

Conjunction of Eqs. (23) and (25) describes, in parametric form, the dependence of C on T for $T>T_{N2}$. Also, Eq. (23) in conjunction with an obvious relation

$$\eta_2=\frac{\sigma+\eta_0}{1-\kappa} \tag{26}$$

describes the temperature variation of the polarization η_2. The parameter σ varies between 0 ($T=\infty$) and σ_N ($T=T_{N2}$), where $\sigma_N=\eta_N(1-\kappa)-\eta_0$ and η_N is defined by Eq. (29) below.

(ii) $\eta\neq 0 (T<T_{N2})$. Equation (12) can be divided by η:

$$\frac{2\,\theta}{\Delta}\tanh\left(\frac{\Delta}{2T}\right)=1. \tag{27}$$

This enables us to eliminate the hyperbolic tangent from Eq. (13):

$$g_y\mu_B H_{\rm ex}+2\,\theta_2\,\eta_2=2\,\theta[(1-\kappa)\,\eta_2-\eta_0], \tag{28}$$

or

$$\eta_2\equiv\eta_N=\frac{g_y\mu_B H_{\rm ex}/2+\theta\,\eta_0}{\theta(1-\kappa)-\theta_2}, \tag{29}$$

i.e., η_2 remains constant from T_{N2} down to 0 K. It is convenient to define parameter σ in this temperature range in such a way as to comply with Eq. (19),

$$\sigma=\tanh\left(\frac{\Delta}{2T}\right)=\frac{\Delta}{2\,\theta}. \tag{30}$$

Then Eq. (20) for the entropy can be used both above and below T_{N2}, $\sigma<\sigma_N$, and $\sigma>\sigma_N$, respectively. Obviously, the entropy is continuous at T_{N2}, where a second-order phase transition takes place.

Substituting Eq. (28) into Eq. (11) and dividing the latter by 2θ, we get the relation between σ and η

$$\sigma=(\eta^2+\sigma_N^2)^{1/2}. \tag{31}$$

It is also convenient to redefine below T_{N2} the dimensionless thermal variable t as follows: $t=T/\theta$ [t was defined above T_{N2} by Eq. (21)]. Then one can make use of Eq. (24) to calculate the specific heat C. The final set of equations describing parametrically the C vs t dependence for $T<T_{N2}$ is

$$t=\frac{2\sigma}{\ln[(1+\sigma)/(1-\sigma)]}, \tag{32}$$

$$C=\frac{\sigma^2(1-\sigma^2)}{t(t-1+\sigma^2)}. \tag{33}$$

The parameter σ varies between σ_N ($T=T_{N2}$) and 1 ($T=0$).

Adding on an obvious relation,

$$\eta=(\sigma^2-\sigma_N^2)^{1/2}, \tag{34}$$

we get the parametric form for η vs T. η increases from $\eta=0$ at $\sigma=\sigma_N$ ($T=T_{N2}$) to a maximum value at $\sigma=1 (T=0)$.

Summarizing, temperature dependence of the electronic polarization of type c_y, η_2, above T_{N2} is described by a pair of parametric equations, Eqs. (23) and (26), where the parameter σ varies between zero ($T=\infty$) and some positive value $\sigma_N<1$, corresponding to T_{N2}. Below T_{N2}, η_2 is constant and equal to η_N, Eq. (29). The quantity η, describing the proper magnetic order of Nd whose exact type is unknown, is zero above T_{N2} and is given by parametric equations (32) and (34) below T_{N2}, $\sigma_N<\sigma<1$. Finally, temperature dependence of the specific heat is found from parametric equations (23) and (25) above T_{N2} ($0<\sigma<\sigma_N$) and (32) and (33) below T_{N2} ($\sigma_N<\sigma<1$). The absolute temperature T equals $t\,\theta_2/(\kappa-1)$ above T_{N2} and $t\,\theta$ below T_{N2}.

B. Polarization of the Nd^{3+} nuclear moments

We shall now proceed to calculate the thermal average of the sum of nuclear spin operators that enters Eqs. (5) and (6). The subsystem of nuclear spins of Nd can be regarded as an ideal paramagnet acted upon by a staggered hyperfine field $H_{\rm hf}$ having the same symmetry as the Nd electronic polarization. Since the latter is overwhelmingly dominated by the c_y mode (see Fig. 6 below), we assume that $H_{\rm hf}$, just like $H_{\rm ex}$, has only a y component, positive on Nd site Nos. 1, 2 and negative on site Nos. 3, 4. The Hamiltonian term which describes the hyperfine interaction in the magnetically ordered state is

$$\hat{H}_{\rm hf} = -g_N \mu_N I_z H_{\rm hf}$$

which splits the nuclear eightfold degeneracy ($I=\frac{7}{2}$) into equally spaced states with an energy difference between each:

$$\Delta_{\rm hf} = g_N \mu_N H_{\rm hf}.$$

Then Eq. (5) simplifies to

$$F^{m+h}(010) = -\frac{4b_{{\rm Nd},i}}{\sqrt{I(I+1)}} IB_I\left(\frac{Ig_N\mu_N H_{\rm hf}}{T}\right), \qquad (35)$$

where $B_I(x)$ is the Brillouin function and g_N is the nuclear splitting factor.

As it will become apparent *a posteriori*, within the temperature range under consideration in the present work, $T > 70$ mK, the argument of the Brillouin function remains small as compared with unity. This enables us to expand the Brillouin function in a power series and keep only the first term linear in $H_{\rm hf}$:

$$F^{m+h}(010) = -\frac{4}{3}\sqrt{I(I+1)} b_{{\rm Nd},i} g_N \frac{\mu_N H_{\rm hf}}{T}. \qquad (36)$$

Finally, as we presumably deal with the natural mixture of Nd isotopes, Eq. (36) should be correspondingly averaged. The result is

$$F^{m+h}(010) = b_{\rm eff}\frac{\mu_N H_{\rm hf}}{T}, \qquad (37)$$

with

$$\begin{aligned} b_{\rm eff} &= -2\sqrt{7}[0.1218 b_i(^{143}{\rm Nd}) g_N(^{143}{\rm Nd}) \\ &\quad + 0.0829 b_i(^{145}{\rm Nd}) g_N(^{145}{\rm Nd})] \\ &= (5.3 \pm 0.7)\times 10^{-13}\ {\rm cm}. \end{aligned}$$

The following values have been used.[18,22]

(i) For ^{143}Nd: natural abundance 12.18%, $I=\frac{7}{2}$, $b_i = 21.1(6)\times 10^{-13}$ cm, $g_N = -0.3076$;

(ii) for ^{145}Nd: natural abundance 8.29%, $I=\frac{7}{2}$, $b_i = 13(7)\times 10^{-13}$ cm, $g_N = 0.190$;

(iii) the other Nd isotopes all have $I=0$.

Negative g factors mean that nuclear spins of both ^{143}Nd and ^{145}Nd are antiparallel to the corresponding nuclear magnetic moments and hence to $H_{\rm hf}$.

The hyperfine contribution to the structure factor of the (100) peak is identical with Eq. (37). We thus can rewrite Eq. (6) as follows:

$$F^{m+h}(100) = a_{\rm eff} g_y \eta_2 + b_{\rm eff}\frac{\mu_N H_{\rm hf}}{T}, \qquad (38)$$

where $a_{\rm eff} = 0.93\times 4\,S\ \alpha = 5.0\times 10^{-13}$ cm ($S=\frac{1}{2}$), $b_{\rm eff}$ is the same as in Eq. (38), and parameter η_2 depends on temperature as described in the previous section.

The subsystem of Nd nuclear spins contributes to the specific heat in the form of a Schottky anomaly due to the thermal population of the eight levels, equally spaced by $\Delta_{\rm hf}$. In the temperature region of interest the same high-temperature approximation as employed for the Brillouin function may be applied to the heat capacity

$$C_n = \frac{\overline{\mu_{\rm eff}^2} H_{\rm hf}^2}{3T^2}, \qquad (39)$$

where

$$\begin{aligned} \overline{\mu_{\rm eff}^2} &= \overline{I(I+1) g_N^2 \mu_N^2} = 15.75\times[0.1218 g_N^2(^{143}{\rm Nd}) \\ &\quad + 0.0829 g_N^2(^{145}{\rm Nd})]\mu_N^2 = 0.229\mu_N^2 \end{aligned}$$

is the mean square of the effective nuclear moment for the natural mixture of Nd isotopes.

V. DETERMINATION OF ADJUSTABLE PARAMETERS

Expressions for the structure factors (37) and (38) contain two adjustable parameters—the y component of the g tensor of Nd, g_y, and the hyperfine field on the Nd nuclei, $H_{\rm hf}$. Further four adjustable parameters—θ, θ_2, $H_{\rm ex}$, and χ_{VV}—are employed in calculating η_2 (Sec. IV A). In this section we shall describe at length the procedure used to fit the experimental data, with particular emphasis on its sequential character, so as to dispel natural doubt as to possible ambiguity caused by the relatively large number of adjustable parameters.

A. Fitting the specific-heat data

We start with the specific-heat data above T_{N2}, i.e., in the region of the Schottky anomaly, and notice that the corresponding equations (23) and (25) contain just one free parameter δ, defined by Eq. (22). Letting σ run from 0.4 to 0.99 with step 0.01, we generated C vs t dependences for a few values of δ; some of them are shown in Fig. 4. The curves have characteristic Schottky-type maxima, the height of which is uniquely determined by δ. Experimentally, the specific heat reaches the maximum value of 0.398 at $T = 2.19$ K[3]. To reproduce this maximum value, δ should be taken equal to 4.3; the maximum is then reached at $t = 2.79$, Fig. 4. Thus, $t = 2.79$ must correspond to $T = 2.19$ K. This sets the coefficient of proportionality between T and t, $\theta_2/(\kappa-1) = 0.785$ K. We can now plot the specific heat against T, rather than against t, which simply means taking the $\delta = 4.3$ curve from Fig. 4 and rescaling the abscissa by a factor of 0.785. The result is the continuous curve in Fig. 5 (to the right from the peak).

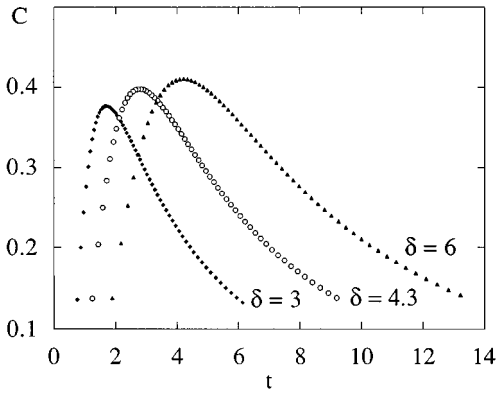

FIG. 4. Dependence of the specific heat on dimensionless temperature, calculated using parametric Eqs. (21) and (23) with $0.4 \leqslant \sigma \leqslant 0.99$, for various fixed values of δ.

We choose the ''model'' Néel point $T_{N2}=1.2$ K, which is slightly higher than the experimental value 1.05 K.[2] (Such discrepancy is inherent in the mean-field approximation, taking a smaller T_{N2} would make the peak too tiny to see. For the compromise value $T_{N2}=1.2$ K, the peak is shifted slightly to the right but it is not too small as compared to the experiment, so the overall agreement is better.) The corresponding dimensionless Néel point is $t_N=1.2/0.785=1.52$, which means that $\sigma_N=0.975$. This latter value can be readily checked by substitution into Eq. (23); the $t(\sigma)$ dependence described thereby is monotonic. At the Néel point one can simultaneously use equations derived for $T>T_{N2}$ and those for $T<T_{N2}$; thus, by virtue of Eq. (30), $\theta=\Delta/2\sigma$, where Δ is given by Eq. (19) with η_2 taken from Eq. (26), and everywhere we set $\sigma=\sigma_N$. This enables us to evaluate θ:

$$\theta=\frac{\theta_2}{\kappa-1}\left(\frac{\delta}{\sigma_N}-1\right)=0.785\times\left(\frac{4.3}{0.975}-1\right)=2.7\ \text{K}.$$

We can finally calculate the low-temperature ($T<T_{N2}$) part of the specific-heat curve, Fig. 5, using Eqs. (32) and (33), where σ runs from $\sigma_N=0.975$ to 1; the absolute temperature T is obtained multiplying t by $\theta=2.7$ K. Summarizing, fitting the electronic contribution to the specific-heat data has

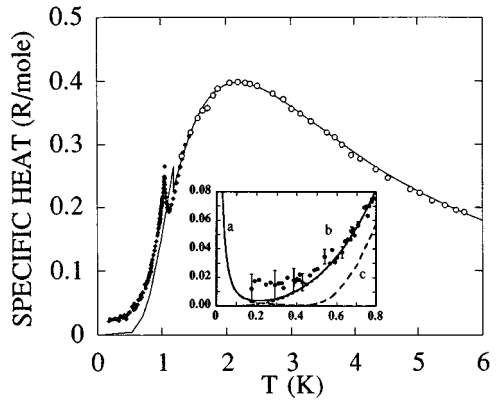

FIG. 5. Temperature dependence of the specific heat of $NdFeO_3$: ♦ experiment, Ref. 2; ○ experiment, Ref. 3; continuous curve—calculation, see the text. Inset; ● low-temperature data. (a) Hyperfine contribution calculated with $H_{\text{hf}}=1$ MOe, (b) spin-wave contribution, (c) mean-field model calculation.

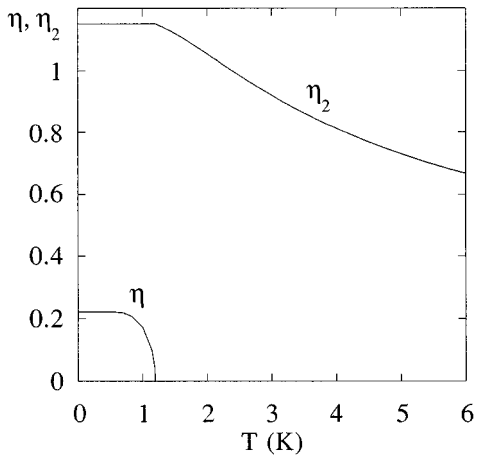

FIG. 6. Calculated temperature dependence of parameters η and η_2.

yielded the following parameters: $\delta=4.3$, $\theta_2/(\kappa-1)=0.785$ K, $\sigma_N=0.975$, $\theta=2.7$ K.

On the other hand, we note in Fig. 5 and curve (c) in its insert that below T_{N2} the mean-field model does not give good account of the experimental data, essentially because this simple model does not consider spin-wave excitations. It is known that the spin-wave contribution for a three-dimensional antiferromagnet is $C/R=AT^3$, and indeed our data may be fitted with the value $A=0.16\ \text{K}^{-3}$ [see inset, curve (b)]. We have included in the inset [curve (a)] the expected hyperfine contribution calculated with the hyperfine field $H_{\text{hf}}=1$ MOe, the value found in the diffraction experiment (see next section) and added it to the spin-wave contribution. We see in Fig. 5(b) that the total predicted curve agrees with the data, within the experimental error. We note, however, that the uncertainty in the data is rather high at the lowest temperatures because the spin-lattice relaxation time increases enormously giving rise to a large scatter in the measured points.

B. Fitting the neutron diffraction data

We shall start with the (100) reflection, Fig. 1. When $T>T_{N2}$, the hyperfine contribution to the structure factor—the second term in Eq. (36)—can be neglected, therefore, $F(100)=a_{\text{eff}}\, g_y\, \eta_2$. Within that range of temperature we are thus left, apart from the obvious scaling factor g_y, with the quantity η_2, whose temperature variation is described parametrically by Eqs. (23) and (26). Equation (26) contains a yet unknown parameter η_0 (the other parameter κ is not in fact independent, since $\eta_0/\kappa=-\delta=-4.3$). Let us take $T'=1.26$ K and $T''=14.6$ K as two reference points. The two corresponding points on the t scale are obtained by division by 0.785: $t'=1.605$ and $t''=18.6$. Finally, $\sigma'=0.969$ and $\sigma''=0.216$ are the respective values of σ, those which yield t' and t'' when substituted into Eq. (23). According to our data, Fig. 1, the structure factor $F(100)$ at T' is 2.72 times greater than it is at T''. Therefore, by virtue of Eq. (26), $\sigma'+\eta_0=2.72(\sigma''+\eta_0)$ or $\eta_0=0.22$. We also get immediately $\kappa=-\delta/\eta_0=-0.051$, $\theta_2=0.785\times(\kappa-1)=-0.825$ K, and $\eta_N=(\sigma_N+\eta_0)/(1-\kappa)=1.14$. The η_2 vs T dependence is now fully determined, see Fig. 6. Then we plot $(a_{\text{eff}}\, g_y\, \eta_2)^2$

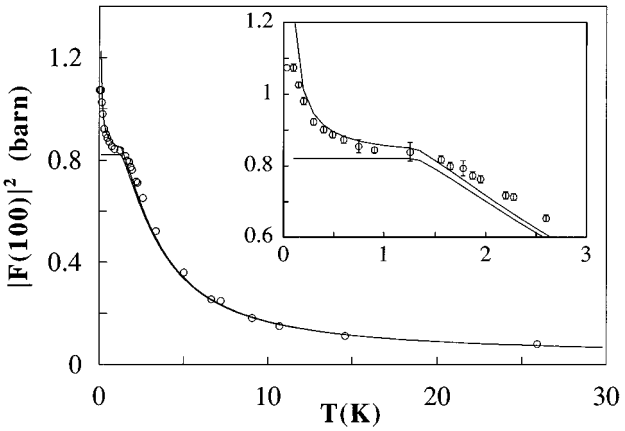

FIG. 7. Temperature dependence of the (100) peak intensity: the points are the experimental data; the lower continuous curve was calculated without the hyperfine contribution [the first term of Eq. (36) only]; the upper continuous curve was calculated using the complete Eq. (36).

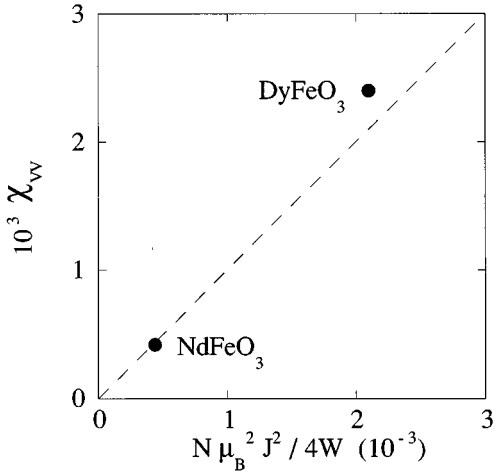

FIG. 8. Comparison of the experimental values of van Vleck susceptibility for $NdFeO_3$ and $DyFeO_3$ perovskites with the estimated dependence on the inverse of the energy gap W (see text).

against temperature and compare it with experimental data. The best agreement is achieved with $g_y=1.6$ (lower continuous curve in Fig. 7).

Let us now consider the (010) reflection, Fig. 3. According to Eq. (37), the structure factor $F(010)$ depends upon just one adjustable parameter, the hyperfine field $H_{\rm hf}$; the best agreement with experiment was obtained for $H_{\rm hf}=1.0\pm0.15$ MOe, the solid curve in Fig. 3. (The large error in $H_{\rm hf}$ comes from our poor knowledge of g_N of ^{145}Nd.) We finally substitute this value of $H_{\rm hf}$ into Eq. (38) and plot the resulting $|F(100)|^2$ across the whole range of temperature (Fig. 7, the upper continuous line). We thus have found the following values for the adjustable parameters of the model: $\theta=2.7$ K, $\theta=-0.825$ K, $H_{\rm ex}=66$ kOe, $\chi_{VV}=4.2\times10^{-4}$, $g_y=1.6$, $H_{\rm hf}=1.0$ MOe.

VI. DISCUSSION

It can be inferred from Figs. 3, 5, and 7 that, with the above parameters, our model gives a fair account for both the specific-heat and the neutron diffraction data under consideration. The salient feature of the model is its allowance for Van Vleck susceptibility. The value that we found, $\chi_{VV}=4.2\times10^{-4}$, can be compared with the low-temperature susceptibility of $DyFeO_3$ along the c axis,[23] 2.4×10^{-3}, which has purely Van Vleck origin due to the special character of the ground state of Dy. Due to the low symmetry of the rare-earth site in the orthoferrites, the wave functions corresponding to the crystal-field levels are generally unknown and exact evaluation of χ_{VV} appears at present impossible. A very crude estimation can be given assuming that at low temperatures only the ground Kramers doublet is populated and that under magnetic field it mixes with the first excited doublet only. Adopting the ''typical'' value $(J/2)\ \mu_B$ for the matrix element between the ground and the first excited doublets we get $\chi_{VV}=N\mu_B^2J^2/4W$, where W is the energy gap separating the doublets [$W=122$ K for $NdFeO_3$ (Ref. 21) and 75 K for $DyFeO_3$ (Ref. 24)]. Despite its roughness, this estimate predicts χ_{VV} surprisingly well, see Fig. 8.

With the value of the hyperfine field now established, $H_{\rm hf}=1.0$ MOe, it can be finally verified that the argument of the Brillouin function in Eq. (35) is 0.56 at the most (for ^{143}Nd at $T=70$ mK). This justifies the expansion of the Brillouin function in Eq. (36) and the use of Eq. (39), whose validity is subject to the same condition.

One can establish a direct correspondence between parameters θ and θ_2 of this work and the exchange integral $J=-0.88(3)$ K found in Ref. 2. Namely, $\theta=2.7$ K$\leftrightarrow-3J=2.64(9)$ K and $\theta_2=-0.825$ K$\leftrightarrow J=-0.88(3)$ K, i.e., the values of our parameters practically coincide with those of their counterparts from Ref. 2 and even though in this work θ and θ_2 are regarded as independent their ratio $\theta/\theta_2\approx-3.3$ does not happen to differ much from -3, as was imposed in Ref. 2. The values of $g_y\mu_BH$ex are also close: 7.1 K in this work and 6.8 K in Ref. 2.

The overall magnetic moment of Nd at $T=1.5$ K (where $\eta_2=1.12$, Fig. 6) is oriented along the b axis and equals $\eta_2g_y/2=0.9\ (\mu_B)$. This value agrees well with what was earlier obtained in powder neutron diffraction experiments,[19] $\mu_y(\mathrm{Nd})=0.92(7)\ \mu_B$. However, the authors of Ref. 19 also report to have detected at $T=1.5$ K a considerable x component of the Nd moment $\mu_x(\mathrm{Nd})=0.68\ \mu_B$, which our model assumes negligibly small. Our point of view can be supported by the following simple consideration. Spontaneous magnetization of polycrystalline $NdFeO_3$ was found to be $\sim0.05\ \mu_B$/f.u. at $T=1.3$ K (Ref. 25), so for a single crystal this value should be about twice as big, i.e., $\sim0.1\ \mu_B$/f.u. This magnetization is oriented along the a axis and consists of negative iron contribution (associated with F_x) $\sim0.05\ \mu_B$/f.u. [independent of temperature and equal to that for $LaFeO_3$ (Ref. 26)] and positive Nd contribution (associated with f_x), which thus appears to be $\sim0.15\ \mu_B$/f.u. at $T=1.3$ K. Therefore, at $T=1.5$ K $\mu_x(\mathrm{Nd})$ should be less than $0.15\ \mu_B$ and it can be neglected. The reason of the erroneously large $\mu_x(\mathrm{Nd})$ in Ref. 19, is not clear at present.

The Zeeman component of the Nd moment at $T=1.5$ K is $\sigma g_y/2=0.75\ (\mu_B)$, i.e., the specific weight of the Van Vleck contribution is about 17%. However, this specific weight grows rapidly with temperature; at $T=6$ K it is already as high as 30%. The Van Vleck contribution to the Nd moments

thus appears quite important for quantitative description of the neutron diffraction peak intensities. However, it does not enter Eq. (20) for the magnetic entropy (which depends only on the Zeeman component of the polarization σ) and hence does not affect the specific heat. For that reason the specific-heat data alone were successfully described in Ref. 2 disregarding the Van Vleck susceptibility.

The low-temperature electronic magnetic moment of Nd $\mu_{\mathrm{Nd}}=0.9\ \mu_B$ is presented in Fig. 8 against the hyperfine field on Nd $H_{\mathrm{hf}}=1.0$ MOe. This moment appears greatly reduced in comparison with the free-ion value 3.27 μ_B. This is characteristic of oxides, where the ground state of the rare earth is formed by the strong crystal field to be peculiar to each individual compound, for example, $\mu_{\mathrm{Nd}}=1.3\ \mu_B$ in $NdCrO_3$ (Ref. 27) and $\mu_{\mathrm{Nd}}=2.8\ \mu_B$ in $NdScO_3$.[33]

A distinct situation takes place in $3d-4f$ intermetallics rich in the $3d$ element: here the $3d$ subsystem is a ferromagnetic producing a strong exchange field acting on the rare earth and making its ground state nearly pure $|JM\rangle$, $M=J$, so that the magnetic moment is close to its free-ion value $g_J J\mu_B$. In line with that, the hyperfine fields on Nd in such compounds (determined by NMR[28,29]) show little variety—they all fall within a narrow interval between 3.45 and 3.60 MOe (see Fig. 9). (The alloy $Nd_{0.1}Gd_{0.9}$ studied in Ref. 30 belongs to this group of compounds too.) However, our results provide evidence in favor of the universal proportionality between the electronic magnetic moment and the hyperfine field on Nd, see Fig. 9.

Unfortunately, we are unable to include in this analysis the data on $NdGaO_3$ (Ref. 16) and Nd_2CuO_4 (Ref. 31), where polarization of Nd nuclear moments was observed as well, because those data were given in arbitrary units. The value of the hyperfine interaction constant which the authors of Ref. 31 deduced from their own data cannot be relied upon either, because (i) a factor $I=\frac{7}{2}$ is missing in their Eq. (5), (ii) the fitting procedure employed in Ref. 31 was ill defined. Chattopadhyay and Siemensmeyer[31] regarded ''const.'' and a_0 as independent parameters in the expression const. $[B_I(a_0 I/T)]^2$, which in their experimental conditions was practically equal to const. $a_0^2 I^2/T^2$ and thus essentially depended only on the product of ''const.'' and a_0^2. The value of ''const.'' was discarded, whereas a_0 alone is worth little.

In regards to the symmetry of the Nd subsystem in the ordered phase, from the outset the possibility of it being Γ_2 was out of the question since the symmetries of the Nd and Fe subsystems must be different. On the basis of our data we can now also eliminate the modes $c_z(\Gamma_1)$ and $c_x(\Gamma_3)$. Indeed, if one of them were present, it would add to $|F^m(010)|^2$ a contribution proportional to $\eta^2(T)$, i.e., practically constant below 0.5 K, and equal to 0.035 b. Figure 3 denies such a suggestion. Finally, the purely ferromagnetic $f_y(\Gamma_3)$ and $f_z(\Gamma_4)$ modes should be rejected too, as being highly unlikely in these antiferromagnetic materials.

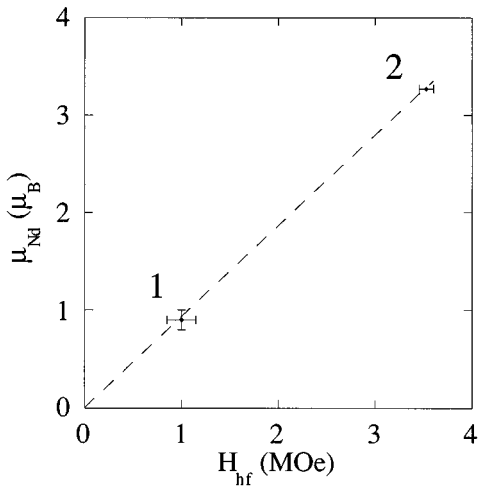

FIG. 9. Electronic moment against hyperfine field on Nd: (1) $NdFeO_3$, this work; (2) Nd intermetallic compounds. The ordinate of point 2 is the free-ion value $\mu_{\mathrm{Nd}}=3.27\ \mu_B$; the horizontal error bar covers the interval with the following experimental data points: $H_{\mathrm{hf}}=3.53$ MOe for Nd_2Fe_{17} and 3.47 MOe for $NdFe_{11}Ti$ (Ref. 29), 3.45 and 3.60 MOe for the two Nd sites in $Nd_2Fe_{14}B$ (Ref. 28), 3.59 MOe for $Nd_{0.1}Gd_{0.9}$ (Ref. 30).

The only admissible magnetic configurations of Nd are the noncentrosymmetric $\Gamma_5-\Gamma_8$, but among them only $\Gamma_5(g_x a_y)$ and $\Gamma_8(a_x g_y)$ are likely to take place in $NdFeO_3$, as they occur in other orthoferrites[32] as well as in isostructural $NdScO_3$ and $NdInO_3$.[33] One could not conceivably observe reflections produced by the modes g, since all of them are superimposed by much stronger nuclear reflections. Thus, the only way to advance by means of single-crystal neutron diffraction would be to look for the (001) line, which may be produced by modes $a_y(\Gamma_5)$ or a_x (Γ_8). It should be noted, however, that the powder neutron diffraction experiments[20] failed to detect the (001) peak.

In conclusion, the type magnetic ordering of Nd in $NdFeO_3$ is in all likelihood Γ_5 or Γ_8. Its observation in a single-crystal neutron diffraction experiment, presents a difficult task.

ACKNOWLEDGMENTS

J.B. and E.P. thank the EU Training and Mobility of Researchers Programme for financial aid in performing the experiments at the Hahn-Meitner-Institut BENSC Reactor. This work was supported by the MAT93/240/C04 CICYT Project. I.S. and R.P. thank the EU for support through the programme PECO93. R.P. thanks the Foundation for Polish Science for their financial support.

[1] W. C. Koehler, E. O. Wollan, and M. K. Wilkinson, Phys. Rev. **118**, 58 (1960).
[2] F. Bartolomé, M. D. Kuz'min, J. Bartolomé, J. Blasco, J. García, and F. Sapiña, Solid State Commun. **91**, 177 (1994).
[3] P. Pataud and J. Sivardière, J. Phys. (France) **31**, 1017 (1970).
[4] S. Geller and E. Wood, Acta Crystalogr. **9**, 563 (1956).
[5] E. F. Bertaut and F. Forrat, J. Phys. Radium **17**, 129 (1956).
[6] E. F. Bertaut, in *Magnetism*, edited by G. T. Rado and H. Suhl (Academic, New York, 1963), Vol. III.
[7] D. Treves, J. Appl. Phys. **36**, 1033 (1965).

[8] K. P. Belov, A. M. Kadomtseva, T. L. Ovchinnikova, V. A. Timofeeva, and V. V. Uskov, Sov. Phys. Solid State, **13**, 518 (1971).
[9] K. P. Belov, M. A. Belkyanchikova, A. M. Kadomtseva, I. B. Krynetskii, T. M. Ledneva, T. L. Ovchinnikova, and V. A. Timofeeva, Sov. Phys. Solid State **14**, 199 (1972).
[10] R. M. Hornreich and I. Yaeger, Int. J. Magn. **4**, 71 (1973).
[11] P. Pataud and J. Sivardière, J. Phys. (France) **31**, 803 (1970).
[12] I. Sosnowska and P. Fischer, Phase Trans. **8**, 319 (1987).
[13] J. D. Cashion, A. H. Cooke, D. M. Martin, and M. R. Wells, J. Phys. C **3**, 1612 (1970).
[14] A. Berton and B. Sharon, J. Appl. Phys. **39**, 1367 (1968).
[15] F. Bartolomé, M. D. Kuz'min, R. I. Merino, and J. Bartolomé, IEEE Trans. Magn. **30**, 960 (1994).
[16] W. Marti, M. Medarde, S. Rosenkranz, P. Fischer, A. Furrer, and C. Klemenz, Phys. Rev. B **52**, 4275 (1995).
[17] L. V. Azároff and M. J. Buerger, *The Powder Method in X-ray Crystallography* (McGraw-Hill, New York, 1958).
[18] *International Tables of Crystallography*, edited by A. J. C. Wilson (Kluwer, Dordrecht, 1992), Vol. C.
[19] R. Przeniosło, I. Sosnowska, and P. Fischer, J. Magn. Magn. Mater. **140-144**, 2153 (1995).
[20] R. Przeniosło, I. Sosnowska, P. Fischer, W. Marti, F. Bartolomé, J. Bartolomé, E. Palacios, and R. Sonntag, J. Magn. Magn. Mater. **160**, 370 (1996).
[21] M. Loewenhaupt, I. Sosnowska, and B. Frick, J. Phys. (France) **49**, C8-921 (1988).
[22] J. M. Spaeth, J. R. Niklas, and R. H. Bartram, *Structural Analysis of Point Defects in Solids* (Springer-Verlag, Berlin, 1992), Appendix A, p. 329.
[23] K. P. Belov, A. K. Zvezdin, A. M. Kadomtseva, and I. B. Krynetskii, Sov. Phys. JETP **40**, 980 (1974).
[24] H. Schuchert, S. Hüfner, and R. Faulhaber, Z. Phys. **220**, 273 (1969).
[25] R. M. Bozorth, H. J. Williams, and D. E. Walsh, Phys. Rev. **103**, 572 (1956).
[26] K. P. Belov, A. K. Zvezdin, A. M. Kadomtseva, and R. Z. Levitin, Sov. Phys. Usp. **19**, 574 (1976).
[27] E. F. Bertaut and J. Mareschal, J. Solid State Commun. **5**, 93 (1967).
[28] Y. Berthier, M. Boge, G. Czjzek, D. Givord, C. Jeandey, H. S. Li, and J. L. Oddou, J. Magn. Magn. Mater. **54-57**, 589 (1986).
[29] C. Kapusta and P. C. Riedi, in *NMR Studies of Intermetallics and Interstitial Solutions Containing H, C and N*. Vol. 281 of *NATO Advanced Studies Institute Series E*: *Interstitial Intermetallic Alloys*, edited by F. Grandjean, G. J. Long, and K. H. J. Buschow (Kluwer, Dordrecht, 1995), Chap. 20.
[30] S. Kobayashi, N. Sano, and J. Ito, J. Phys. Soc. Jpn. **21**, 1456 (1966).
[31] T. Chattopadhyay and K. Siemensmeyer, Europhys. Lett. **29**, 579 (1995).
[32] K. P. Belov, A. K. Zvezdin, and A. M. Kadomtseva, *Rare-Earth Orthoferrites, Symmetry and Non-Heisenberg Exchange*. Vol. 9 of *Soviet Science Reviews, Series A*: *Physics Reviews*, edited by I. M. Khalatnikov (Harwood, Chur, Switzerland, 1987), p. 117.
[33] I. Plaza, E. Palacios, J. Bartolomé, A. Furrer, S. Rosenkranz, and C. Ritter, Physica B (to be published).